

Strain drived band aligment transition of the ferromagnetic VS_2/C_3N van der Waals heterostructure

Jimin Shang(商继敏), Shuai Qiao(乔帅), Jingzhi Fang(房景治), Hongyu Wen(文宏玉), and Zhongming Wei(魏钟鸣)

Citation: Chin. Phys. B, 2021, 30 (**9**): 097507. DOI: 10.1088/1674-1056/ac0cd1
Journal homepage: http://cpb.iphy.ac.cn; http://iopscience.iop.org/cpb

What follows is a list of articles you may be interested in

Magnetic dynamics of two-dimensional itinerant ferromagnet Fe_3GeTe_2

Lijun Ni(倪丽君), Zhendong Chen(陈振东), Wei Li(李威), Xianyang Lu(陆显扬), Yu Yan(严羽), Longlong Zhang(张龙龙), Chunjie Yan(晏春杰), Yang Chen(陈阳), Yaoyu Gu(顾耀玉), Yao Li(黎遥), Rong Zhang(张荣), Ya Zhai(翟亚), Ronghua Liu(刘荣华), Yi Yang(杨燚), and Yongbing Xu(徐永兵)

Chin. Phys. B, 2021, 30 (**9**): 097501. DOI: 10.1088/1674-1056/ac0e25

Electric-field-induced in-plane effective 90° magnetization rotation in Co_2FeAl/PMN-PT structure

Cai Zhou(周偲), Dengyu Zhu(朱登玉), Fufu Liu(刘福福), Cunfang Feng(冯存芳), Mingfang Zhang(张铭芳), Lei Ding(丁磊), Mingyao Xu(许明耀), and Shengxiang Wang(汪胜祥)

Chin. Phys. B, 2021, 30 (**5**): 057504. DOI: 10.1088/1674-1056/abd7de

Spin correlations in the *S=1* armchair chain Ni_2NbBO_6 as seen from NMR

Kai-Yue Zeng(曾凯悦), Long Ma(马龙), Long-Meng Xu(徐龙猛), Zhao-Ming Tian(田召明), Lang-Sheng Ling(凌浪生), and Li Pi(皮雳)

Chin. Phys. B, 2021, 30 (**4**): 047503. DOI: 10.1088/1674-1056/abc2b5

Origin of itinerant ferromagnetism in two-dimensional Fe_3GeTe_2

Xi Chen(陈熙), Zheng-Zhe Lin(林正喆), and Li-Rong Cheng(程丽蓉)

Chin. Phys. B, 2021, 30 (**4**): 047502. DOI: 10.1088/1674-1056/abd164

Magnetic anisotropy in 5d transition metal-porphyrin molecules

Yan-Wen Zhang(张岩文), Gui-Xian Ge(葛桂贤), Hai-Bin Sun(孙海斌), Jue-Ming Yang(杨觉明), Hong-Xia Yan(闫红霞), Long Zhou(周龙), Jian-Guo Wan(万建国), and Guang-Hou Wang(王广厚)

Chin. Phys. B, 2021, 30 (**4**): 047501. DOI: 10.1088/1674-1056/abcf9c

---

SPECIAL TOPIC — Two-dimensional magnetic materials and devices

Strain drived band aligment transition of the ferromagnetic VS_2/C_3N van der Waals heterostructure*

Jimin Shang(商继敏)[1], Shuai Qiao(乔帅)[1], Jingzhi Fang(房景治)[2], Hongyu Wen(文宏玉)[2,†], and Zhongming Wei(魏钟鸣)[2]

[1] School of Physics and Electronics Engineering, Zhengzhou University of Light Industry & Henan Key Laboratory of Magnetoelectronic Information Functional Materials, Zhengzhou University of Light Industry, Zhengzhou 450002, China

[2] State Key Laboratory of Superlattices and Microstructures, Institute of Semiconductors, Chinese Academy of Sciences & Center of Materials Science and Optoelectronics Engineering, University of Chinese Academy of Sciences, Beijing 100083, China

(Received 25 April 2021; revised manuscript received 17 June 2021; accepted manuscript online 21 June 2021)

Exploring two-dimensional (2D) magnetic heterostructures is essential for future spintronic and optoelectronic devices. Herein, using first-principle calculations, stable ferromagnetic ordering and colorful electronic properties are established by constructing the VS_2/C_3N van der Waals (vdW) heterostructure. Unlike the semiconductive properties with indirect band gaps in both the VS_2 and C_3N monolayers, our results indicate that a direct band gap with type-II band alignment and p-doping characters are realized in the spin-up channel of the VS_2/C_3N heterostructure, and a typical type-III band alignment with a broken-gap in the spin-down channel. Furthermore, the band alignments in the two spin channels can be effectively tuned by applying tensile strain. An interchangement between the type-II and type-III band alignments occurs in the two spin channels, as the tensile strain increases to 4%. The attractive magnetic properties and the unique band alignments could be useful for prospective applications in the next-generation tunneling devices and spintronic devices.

Keywords: two-dimensional ferromagnetic material, van der Waals heterostructure, band alignment, strain

PACS: 75.70.Cn, 61.82.Fk **DOI:** 10.1088/1674-1056/ac0cd1

1. Introduction

Two-dimensional (2D) materials have been regarded as prospective candidates on account of the outstanding properties.[1–4] However, single 2D material does not possess perfect properties for practical applications, such as the zero-band gap of graphene limiting its applications in optoelectronic devices. Accordance with prior research, constructing van der Waals (vdW) heterostructure is purposefully carried out together to obtain many new properties beyond single components.[5–8] Nevertheless, the existing vdW heterostructures with the intrinsic ferromagnetic (FM) properties are rare. To develop the application of vdW heterostructures in spintronics, as well as memory and storge devices, the explorations of magnetic properties in vdW heterostructures are essential. Due to majority 2D materials are nonmagnetic, many methods to induce magnetic ordering have focused on the doping, defect, application of electric fields, and surface functionalization.[9–12] However, the external modulation would lead to the complex correlation of the orbital and the lattice. Since the long-range magnetic order was observed in $Cr_2Ge_2Te_6$ and CrI_3,[13,14] many novel phenomena and 2D magnetic materials have been reported. While the lacking of FM vdW heterostructures to date hinders the uses of 2D materials in spintronic devices. Therefore, it is highly desirable to explore new 2D magnetic vdW heterostructures to extend their multifunctional applications.

Recently, as a new member of 2D transition-metal dichalcogenides (TMDs) family, the atomically vanadium disulfde (VS_2) monolayer is confirmed to have an intrinsic FM semiconducting property,[15,16] which could be a suitable candidate for constructing 2D magnetic vdW heterostructures. Xiong *et al.* reported that the $Mg(OH)_2/VS_2$ heterostructure possesses the FM properties with high Curie temperature.[17] Du *et al.* theoretically predicted that a half-metal state with 100% spin-polarized currents could be obtained by applying an electronic field in $MoS_2(WS_2)/VS_2$ vdW heterostructures.[18] However, the previous reports on the 2D atomically thin vdW heterostructures based on VS_2 are rare. As the 2D FM heterostructures have great potential application of nanoelectronic and spintronic devices, more FM vdW heterostructures based on VS_2 with desired properties should be designed. As a typical CN compound, C_3N monolayer has recently been fabricated with remarkable electronic and optoelectronic properties.[19,20] Due to a wide spectral responsive range, C_3N has its potential utilization in photocatalysis and various applications.[21–23] The C_3N monolayer also has many excellent properties similar to graphene, for instance the high carrier mobility and high thermal conductivity.[21,24,25] Thus, the C_3N monolayer will be an outstanding candidate for applications in electronic de-

*Project supported by the National Key Research and Development Program of China (Grant No. 2017YFA0207500), Natural Science Foundation of Henan Province, China (Grant No. 202300410507), and Key Research & Development and Promotion Projects in Henan Province, China (Grant No. 212102210134).

†Corresponding author. E-mail: wenhongyu@semi.ac.cn

© 2021 Chinese Physical Society and IOP Publishing Ltd

vices due to its suitable band gap, that is very different from graphene.[26] Interestingly, from the previous theoretical results, there is a good lattice match between the 3×3 supercell of VS_2 and the 2×2 of C_3N. Therefore, the VS_2/C_3N would be conveniently prepared in experiments. In addition, VS_2/C_3N would be a magnetic heterostructure with suitable band gap, and should enhance the performance in practical spintronic devices.

According to the above statement, in this work, we construct the VS_2/C_3N van der Waals heterostructures, and discuss the electronic and magnetic properties of the heterostructures. Our first-principles results show that VS_2/C_3N heterostructures exhibit FM semiconducting ground states with multiple band alignments. Particularly, the intrinsic type III alignment indicates that the VS_2/C_3N vdW heterostructure is quite favorable for tunneling and spintronic devices. While the type-II band alignment in the spin-up channel can naturally realize p doping in the heterostructure, and the band alignments also can be tuned by an external strain. Our result provides the multiple electronic and magnetic properties of the heterostructures, which will be very attractive to the potential applications of 2D FM semiconducting heterostructures in electronic and spintronic devices.

2. Methods

Our simulations are all carried out based on the spin-polarized density functional theory (DFT) by employing the Vienna *ab initio* simulation package (VASP) code.[27] The exchange–correlation functional is described using the generalized gradient approximation (GGA) within the Perdew–Burke–Ernzerhof (PBE) formula.[28] The projector-augmented wave (PAW) method[29] is modeled for the core electrons. Moreover, to correct the correlation effects between the localized V-3d electrons, we adopt Dudarev's approach with the on-site Coulomb energy $U = 2$ eV and exchange parameter $J = 0.87$ eV in the spin-polarized DFT+U calculations.[30] The values for V 3d electrons have been checked to yield reliable results in existing theoretical works.[31–33] We also consider the interactions of the VS_2/C_3N vdW heterostructure using the DFT-D2 method of Grimme.[34,35] The plane-wave basis energy cutoff is set to 500 eV. The geometry structures are fully relaxed until the Hellmann–Feynman atomic force on each atom is less than 0.01 eV/Å, and the total energy convergence criterion for electronic iterations is chosen as 10^{-5} eV. In addition, the Monkhorst–Pack method in the Brillouin zone is sampled by $13 \times 13 \times 1$ for the geometry optimization of the system. A vacuum slab of 20 Å along the z-axis is sufficient to avoid the interaction between layers and their periodic images.

3. Results and discussion

To construct the geometric model of the VS_2/C_3N heterostructures, we firstly discuss the structural parameters, electronic and magnetic properties of the VS_2 monolayer and C_3N monolayer. Here we choose the most stable trigonal prismatic (2H) phase of VS_2 monolayer as shown in Fig. 1. The honeycomb structure of 2H-VS_2 consists of two hexagonal atomic layers where the V atomic layer is sandwiched by the two S atomic layers. At the same time, C_3N monolayer has the hexagonal graphene-like structure with one N atom surrounded by three C atoms, which can be regarded as a N-doped graphene. Based on the minimization of the total energy, the optimized lattice parameter is 3.19 Å for VS_2 monolayer, meanwhile is 4.86 Å for monolayer C_3N. Our results are in good agreement with the existing theoretical and experimental data.[17,18,36–38] In order to obtain the very small lattice mismatch, the 3×3 supercell of VS_2 monolayer and 2×2 supercell of C_3N monolayer are proposed to form the VS_2/C_3N vdW heterostructures. The lattice mismatch is also calculated using the formula $\Delta = 2(a_1 - a_2)/(a_1 + a_2)$, where a_1 and a_2 are the lattice constants of the two isolated monolayers, respectively. Here the lattice mismatch is very tiny ($\sim 1.6\%$), which is beneficial for experimentally fabricating VS_2/C_3N vdW heterostructures.

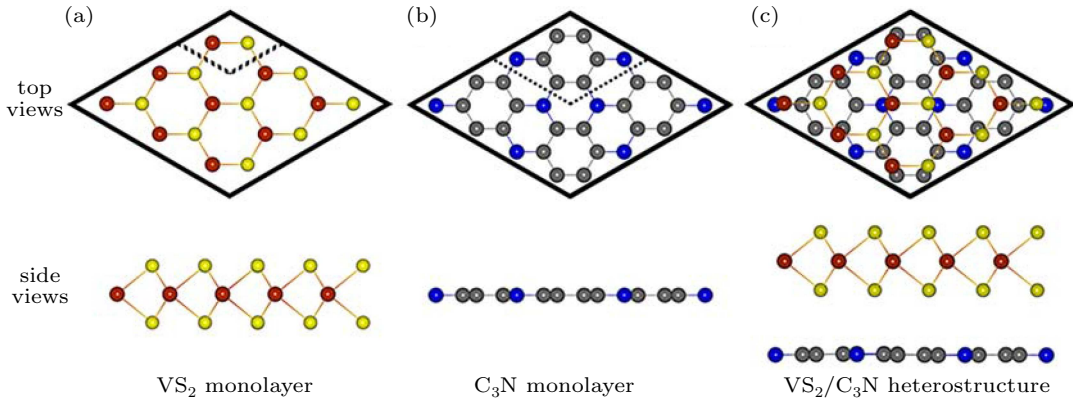


Fig. 1. (a)–(b) The top and side views of the VS_2 and C_3N monolayers. (c) Top and side views of VS_2/C_3N vdW heterostructure. The dashed rhombic frames represent the primitive cells, and the solid frame presents the 3×3 supercell of VS_2 monolayer and 2×2 C_3N monolayers, respectively. The red, yellow, blue, and grey balls represent the V, S, N, C atoms, respectively.

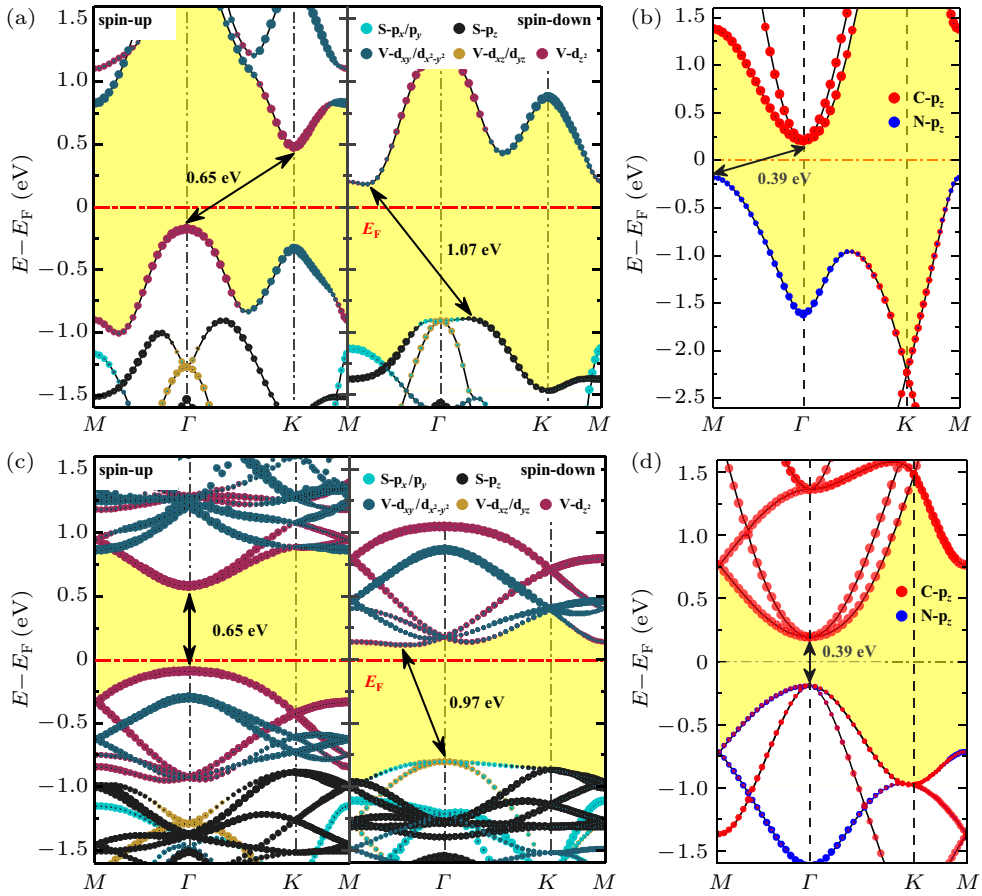


Fig. 2. Orbital resolved band structures of monolayers (a) VS_2 and (b) C_3N calculated with unit cell, (c) VS_2 calculated with 3×3 supercell, (d) C_3N calculated with 2×2 supercell. The Fermi energy level is shifted to 0.0 eV and the sizes of symbols represent contributions from different orbitals.

The orbital resolved band structures of monolayer VS_2 and monolayer C_3N are both obtained using unit cells shown in Figs. 2(a) and 2(b), respectively. The electronic structures of VS_2 monolayer indicate that the most stable FM ordering with 1.0 μ_B magnetic moment on V atom in unit cell can be observed. Therefore, the 3×3 supercell of VS_2 monolayer possesses 9.0 μ_B magnetic moments as shown in Fig. 2(c). The VS_2 monolayer has an indirect bandgap of 0.65 eV with spin up, while the spin down band gap is 0.97 eV, which are consistent with the previous results.[17,18] From the orbital resolved band structures of monolayers VS_2, the CBM and the VBM both are mainly contributed by the V d_{z^2} orbitals. In the spin-down channel, the CBM is composed by V d_{z^2} mixed with V $d_{xy}/d_{x^2-y^2}$ electrons, and the VBM is mainly contributed by S p_z and S p_x/p_y orbitals. For C_3N monolayer, the VBM locates at M point while the CBM locates at Γ. Thus, the indirect bandgap is 0.39 eV, which agrees with previous reports.[37,38] On the other hand, it should be mentioned that the M point in the primitive cell is folded into the Γ point in the 2×2 supercell of the C_3N monolayer. Then as shown in Fig. 2(d), C_3N monolayer presents a direct band gap characteristic in the 2×2 supercell, which has been realized in the previous literatures.[39–41] Similar to the folded band structure in C_3N supercell, the VS_2 monolayer possesses a different band structure in 3×3 supercell from the unit cell as shown in Fig. 2(c). Therefore, the C_3N monolayer and the VS_2 monolayer both emerge the characteristic of direct band gaps in the VS_2/C_3N vdW heterostructure due to the shrinkage of the Brillouin zone.[39,40]

By stacking the 3×3 supercell of VS_2 and 2×2 supercell of C_3N vertically together, the VS_2/C_3N vdW heterostructure is constructed as shown in Fig. 1(c). In our optimized heterostructure, the VS_2 and C_3N still preserve their pristine geometric structures. The lattice parameter of the VS_2/C_3N vdW heterostructure is found to be 9.65 Å, between that of the VS_2 and C_3N monolayers. Using the structural relaxation for the VS_2/C_3N heterostructure, the equilibrium interlayer distance is optimized to be $\sim$ 3.32 Å, which is defined as the vertical distance between the bottom S atomic layer in VS_2 and the C_3N layer. In addition, when biaxial strain (in-plane) is applied, we still adopt the structural relaxation for each atom. From the results of the structural optimization, we find that the interlayer distance is unchanged with the applied in-plane strain. Thus, the interlayer distance remains unchanged in this paper. To further confirm the stability of the heterostructure, we also calculate the binding energy (E_b) using the formula

$$E_b = (E_{VS_2/C_3N} - E_{VS_2} - E_{C_3N})/S, \quad (1)$$

where E_{VS_2/C_3N}, E_{VS_2}, and E_{C_3N} are the total energies of the

VS_2/C_3N, VS_2, and C_3N monolayers, respectively. The S is the interfacial area between VS_2 and C_3N in the heterostructure. The E_b value is found to be -27 meV/Å^2, which demonstrates the weak vdW interactions between the C_3N and VS_2 layers.

Next, we explore the electronic properties of the VS_2/C_3N heterostructure. Figure 3(a) shows the projected band structures of the VS_2/C_3N vdW heterostructure. A direct band gap is realized in the spin-up channel of the VS_2/C_3N heterostructure. The red and blue dots indicate contributions from the VS_2 and C_3N layers, respectively. It can be seen that the stable FM properties are still kept in the VS_2/C_3N heterostructure, while the electronic structures in the spin-up and spin-down channels have an obvious modification comparison with those of the monolayers. The results indicate that the magnetic moment for the VS_2/C_3N vdW heterostructure is 0.9135 μ_B and the magnetic moment of the heterostructure is slightly decreased compared with the magnetic moment of the unit cell (~ 0.9999 μ_B) in the VS_2 monolayer. In the spin-up channel, the CBM and VBM are contributed by the VS_2 and C_3N layers, respectively, exhibiting a typical type-II band alignment. In addition, as shown in Fig. 3(a), the Fermi level crosses the valence band, demonstrating a p-doping character in the C_3N layer. The results indicate a charge (electron) transfer from the C_3N layer to the VS_2 layer by composing VS_2/C_3N heterostructure, which can also be verified by comparing the work functions between the isolated VS_2 and C_3N monolayers. The work functions of the C_3N and VS_2 monolayers are 2.96 eV and 5.87 eV, which indicates that the highest Fermi level lies in C_3N monolayer comparing with VS_2 monolayer both in the spin-up and spin-down channels. Thus, the electrons will flow from the C_3N to the VS_2 monolayer, yet the holes transfer in the opposite direction until forming an equilibrium heterostructure. Therefore, the VS_2/C_3N vdW heterostructure displays an intrinsic type-II band alignment and p-doping characters in the spin-up channel, and the electrons and holes are respectively localized in the VS_2 and C_3N layers, which is favorable for the practical optoelectronic devices. In comparison, a typical type-III band alignment is established in the spin-down channel, which indicates that the VS_2/C_3N vdW heterostructure is a broken gap vdW heterostructure with FM properties. As we know, the broken-gap heterostructures is suitable for the tunneling devices. Due to that there are considerable carrier migration in VS_2/C_3N heterostructures with no external electric field, it will result in an accumulation of electrons in the VS_2 layer and holes in C_3N layer near the junction. Based on the separately accumulation of the carrier, a highly doped p^+/n^+ heterojunction can be obtained in the VS_2/C_3N vdW heterostructure with no electrostatic or chemical doping. This special feature makes VS_2/C_3N heterostructure as an excellent material for negative differential resistance (NDR) devices.[38,42]

To discuss the magnetic properties of the VS_2/C_3N vdW heterostructure, the spin densities of the heterostructure are shown in Fig. 4. We study the ground state magnetic properties of the heterostructure comparing all the possible magnetic orderings. The FM, non-magnetic (NM), and anti-ferromagnetic (AFM) are all calculated using a 2×2 supercell of the heterostructure, containing 36 V atoms. It can be seen that the magnetic moment of the heterostructure is mainly localized on the V atoms. The optimized configurations, local magnetic arrangements, magnetic moments, and energy are all shown in

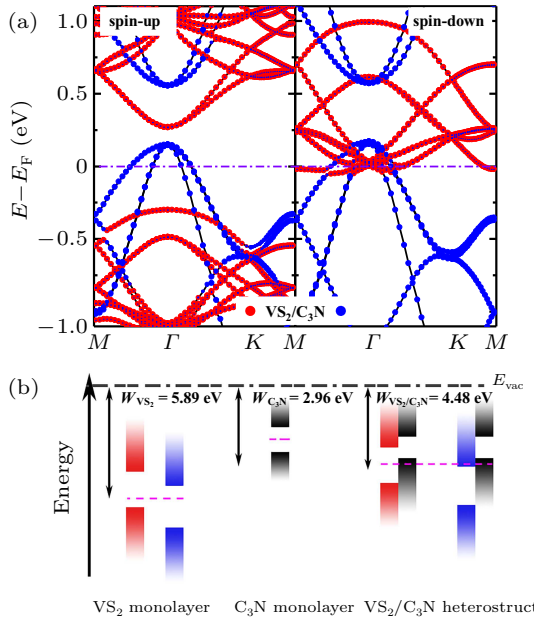


Fig. 3. (a) Projected band structure of VS_2/C_3N vdW heterostructure. The red and blue dots indicate contributions from VS_2 and C_3N monolayers, respectively. (b) Band alignment and work functions of VS_2, C_3N monolayers and VS_2/C_3N heterostructures. The E_{vac} is referred to the vacuum level.

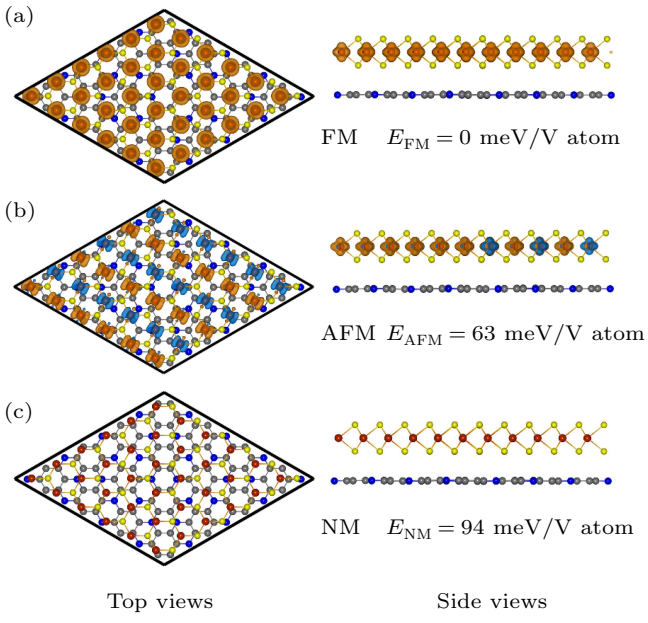


Fig. 4. Spin densities of FM-, AFM1-, AFM2-, and NM-VS_2/C_3N heterostructure. The red and blue colors indicate the spin-up and spin-down sates, respectively.

Fig. 4 for NM, FM, and AFM states, respectively, with respect to the FM configuration (the energy of FM configuration is set to 0). Our numerical results indicate that the AFM ordering has the total energy of $E_{\rm AFM} - E_{\rm FM} \approx 63$ meV/V atom, and NM states has that of $E_{\rm NM} - E_{\rm FM} \approx 94$ meV/V atom, thus the FM ordering is found to be most stable compared with the AFM and NM ones. As a result, the VS_2/C_3N heterostructure presents the FM ground states, which indicates that the VS_2/C_3N heterostructure is a promising candidate for the application of the next-generation spintronic and optoelectronic devices.

It has been proved that strain engineering is an efficient method to modulate the electronic and transport properties in the practical 2D electronic devices, and the practical strain engineering is feasible to induce different compressive and tensile strains by bending the flexible substrate.[43] We also consider applying the strain to the VS_2/C_3N vdW heterostructure. To explore the strain effects on the electronic properties of the heterostructure, we apply the in-plane biaxial strains to VS_2/C_3N heterostructures. In this work, we just focus on the effect of the applied proper strains on their electronic properties, and the range of our considered strain can be easily achieved in the practical strain engineering. The biaxial strain is defined as $\varepsilon = (a - a_0)/a_0 \times 100\%$, where a_0 (9.65 Å) is the lattice constant of the VS_2/C_3N vdW heterostructure in its equilibrium state, and a is the lattice constant of the strained VS_2/C_3N heterostructure. As shown in Figs. 5(a)–5(c), it is clear that tensile strain is a more efficient to modulate the band alignment of the VS_2/C_3N vdW heterostructures both in the spin-up and spin-down channels. From the projected band structure of the heterostructure in Fig. 5, the feature of the C_3N layer is not apparent with the small tensile strain, but the VS_2 layer presents obvious effect under the same tensile strain. In the spin-up channel, the intrinsic type-II band alignment can be tuned into type-III band alignment when the tensile strain is 2%. Meanwhile, a doped p heterojunction is always hold. When the tensile strain reaches 4%, the heavy doped p^+/n^+ heterojunction can be naturally realized in the spin-up channel. Based on the previous literature,[44] the 4% tensile strain will not induce the phase transition of the VS_2 monolayer. Comparing with Figs. 5(a) and 5(c) in the spin-up channel, the CBM (consisted of VS_2 monolayer) in the spin-up channel moves down and crosses the Fermi level, thus the type-II band alignment is turned into type-III. On the other hand, in the spin-down channel the band alignment can also been modulated by the tensile strain. The intrinsic band alignment in the spin-down channel with no strain is type-III. However, when the tensile strain reaches to 4%, the CBM moves far from the Fermi level, and the type-II band alignment with p doping can be obtained in the spin-down channel. In addition, it can be seen from the projected band structure in Fig. 5 that the characteristic of the p doping is always preserved with applying the tensile strain. Namely, the band alignments in the two spin channels can be effectively tuned by applying tensile strain, and an interchangement between the type-II and type-III band alignments can be realized.

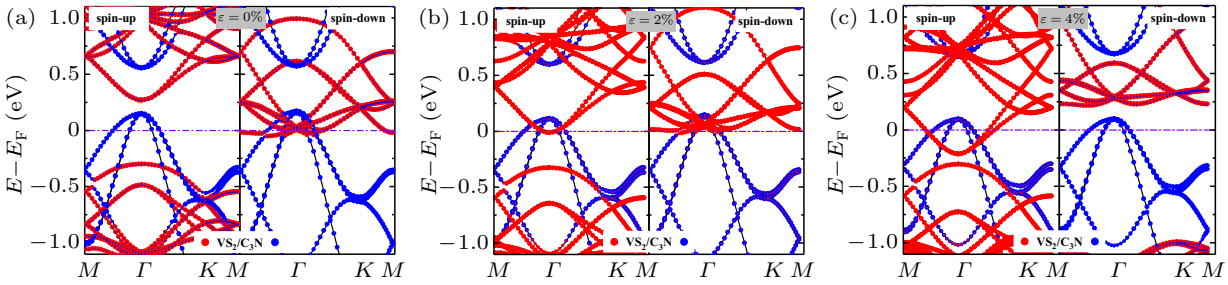


Fig. 5. Evolution of the projected band structures of VS_2/C_3N heterostructure with different in-plane biaxial strains.

4. Conclusion

We discuss the electric and FM properties of the VS_2/C_3N van der Waals heterostructure. The results present that stable ferromagnetic ordering and colorful electronic properties are established by constructing the VS_2/C_3N vdW heterostructure. Different from the monolayers, the VS_2/C_3N heterostructure presents a direct band gap with type-II band alignment and p-doping characters in the spin-up channel of the VS_2/C_3N heterostructure, which indicate that VS_2/C_3N FM heterostructures are fit for a high-efficiency optoelectronic application. On the other hand, a typical type-III band alignment with a broken-gap in the spin-down channel makes it a promising material for tunneling devices. Furthermore, the tuning properties can be induced by applying tensile strain. An interchangement between the type-II and type-III band alignments can be realized in the two spin channels with proper tensile strain. The attractive magnetic properties and the unique band alignments can provide multiple ways to utilize new FM heterostructures in future spintronic and optoelectronic devices.

References

[1] Dean C R, Young A F, Meric I, Lee C, Wang L, Sorgenfrei S, Watanabe K, Taniguchi T, Kim P, Shepard K L and Hone J 2010 *Nat. Nanotechnol.* **5** 722
[2] Hong X P, Kim J and Shi S F 2014 *Nat. Nanotechnol.* **9** 682

[3] Bonilla M, Kolekar S, Ma Y, Diaz H C, Kalappattil V, Das R, Eggers T, Gutierrez H R, Phan M H and Batzill M 2018 *Nat. Nanotechnol.* **13** 289

[4] O'Hara D J, Zhu T, Trout A H, Ahmed A S, Luo Y K, Lee C H, Brenner M R, Rajan S, Gupta J A, McComb D W and Kawakami R K 2018 *Nano Lett.* **18** 3125

[5] Shang J M, Pan L F, Wang X T, Li J B, Deng H X and Wei Z M 2018 *J. Mater. Chem. C* **6** 7201

[6] Liang S J, Cheng B, Cui X and Miao F 2020 *Adv. Mater.* **32** 1903800

[7] Shang J M, Zhang S, Wang Y Q, Wen H Y and Wei Z M 2019 *Chin. Opt. Lett.* **17** 020010

[8] Tan X Y, Liu L L and Ren D H 2020 *Chin. Phys. B* **29** 076102

[9] González-Herrero H, Gómez-Rodríguez J M, Mallet P, Moaied M, Palacios J J, Salgado C, UgedaM M, Veuillen J Y, Yndurain F and Brihuega I 2016 *Science* **352** 437

[10] Li B, Xing T, Zhong M, Huang L, Lei N, Zhang J, Li J and Wei Z 2017 *Nature Commun.* **8** 1958

[11] Ge J, Luo T, Lin Z, Shi J, Liu Y, Wang P, Zhang Y, Duan W and Wang J 2021 *Adv. Mater.* **33** 2005465

[12] Zhou J, Wang Q, Sun Q and Jena P 2010 *Phys. Rev. B* **81** 085442

[13] Gong C, Li L, Li Z, Ji H, Stern A, Xia Y, Cao T, Bao W, Wang C, Wang Y, Qiu Z Q, Cava R J, Louie S G, Xia J and Zhang X 2017 *Nature* **546** 265

[14] Huang B, Clark G, Navarro-Moratalla E, Klein D R, Cheng R, Seyler K L, Zhong D, Schmidgall E, McGuire M A, Cobden D H, Yao W, Xiao D, Jarillo-Herrero P and Xu X 2017 *Nature* **546** 270

[15] Ma Y, Dai Y, Guo M, Niu C, Zhu Y and Huang B 2012 *ACS Nano* **6** 1695

[16] Zhuang H L and Hennig R G 2016 *Phys. Rev. B* **93** 054429

[17] Xiong W, Xia C, Du J, Wang T, Zhao X, Peng Y, Wei Z and Li J 2017 *Phys. Rev. B* **95** 245408

[18] Du J, Xia C, Xiong W, Wang T, Jia Y and Li J 2017 *Nanoscale* **9** 17585

[19] Yang S, Li W, Ye C, Wang G, Tian H, Zhu C, He P, Ding G, Xie X, Liu Y, Lifshitz Y, Lee S, Kang Z and Jiang M 2017 *Adv. Mater.* **29** 1605625

[20] Mahmood J, Lee E K, Jung M, Shin D, Choi H J, Seo J M, Jung S M, Kim D, Li F, Lah M S, Park N, Shin H J, Oh J H and Baek J B 2016 *Proc. Natl. Acad. Sci. USA* **113** 7414

[21] Mortazavi B 2017 *Carbon* **118** 25

[22] Bafekry A, Farjami Shayesteh S and Peeters F M 2019 *J. Phys. Chem. C* **123** 12485

[23] Xu J T, Mahmood J, Dou Y H, Dou S X, Li F, Dai L M and Baek J B 2017 *Adv. Mater.* **29** 1702007

[24] Makaremi M, Mortazavi B and Singh C V 2017 *J. Phys. Chem. C.* **121** 18575

[25] Mouri S, Miyauchi Y and Matsuda K 2013 *Nano Lett.* **13** 5944

[26] Zhou X, Feng W, Guan S, Fu B, Su W and Yao Y 2017 *J. Mater. Res.* **32** 2993

[27] Kresse G and Furthmüller J 1996 *Phys. Rev. B* **54** 11169

[28] Perdew J P, Burke K and Ernzerhof M 1996 *Phys. Rev. Lett.* **77** 3865

[29] Kresse G and Joubert D 1999 *Phys. Rev. B* **59** 1758

[30] Dudarev S L, Botton G A, Savrasov S Y, Humphreys C J and Sutton A P 1998 *Phys. Rev. B* **57** 1505

[31] Ma X, Yin L, Zou J, Mi W and Wang X 2019 *J. Phys. Chem. C* **123** 17440

[32] Luo N, Si C and Duan W 2017 *Phys. Rev. B* **95** 205432

[33] Fuh H R, Chang C R, Wang Y K, Evans R F L, Chantrell R W and Jeng H T 2016 *Sci. Rep.* **6** 32625

[34] Grimme S 2006 *J. Comput. Chem.* **27** 1787

[35] Kerber T, Sierka M and Sauer J 2008 *J. Comput. Chem.* **29** 2088

[36] Slassi A and Cornil J 2018 *2D Mater.* **6** 015025

[37] Tagani M B 2018 *Comput. Mater. Sci.* **153** 126

[38] Yang Y X and Wang Z G 2019 *RSC Adv.* **9** 19837

[39] Xie L, Yang L, Ge W, Wang X and Jiang J 2019 *Chem. Phys.* **520** 40

[40] Wang X, Li Q, Wang H, Gao Y, Hou J and Shao J 2018 *Phys. B* **537** 314

[41] Gao X, Shen Y, Ma Y, Wu S and Zhou Z 2019 *Appl. Surf. Sci.* **479** 1098

[42] Yan R, Fathipour S, Han Y, Song B, Xiao S, Li M, Ma N, Protasenko V, Muller D A, Jena D and Xing H G 2015 *Nano Lett.* **15** 5791

[43] Zhang H, Li Y, Yang M, Zhang B, Yang G, Wang S and Wang K 2015 *Chin. Phys. B* **24** 077501

[44] Kan M, Wang B, Lee Y H and Sun Q 2015 *Nano Research* **8** 1348